Variable-Energy Photoelectron Spectroscopy of (η^5-C_5H_5)NiNO: Molecular Orbital Assignment and Xα−SW Calculations

Xiaorong Li,[†] J. S. Tse,[‡] G. M. Bancroft,*[,†,§] R. J. Puddephatt,*[,†] and K. H. Tan[§]

Department of Chemistry, The University of Western Ontario, London, Canada N6A 5B7, Canadian Synchrotron Radiation Facility, Synchrotron Radiation Centre, University of Wisconsin−Madison, Stoughton, Wisconsin 53589, and Steacie Institute for Molecular Sciences, National Research Council of Canada, Ottawa, Ontario, Canada K1A 0R6

Received July 25, 1995[⊗]

Variable-energy valence and inner-valence photoelectron spectra have been recorded for the CpNiNO complex (Cp = η^5-C_5H_5) between 21.2 and 100 eV, using He I radiation and synchrotron radiation. The ground state electronic structure has been calculated by using the Xα−SW method. Photoionization cross sections (σ) have also been calculated for the valence ionizations using the Xα−SW method. The theoretical branching ratios ($\sigma_i/\sum\sigma$) have been compared with the observed branching ratios ($A_i/\sum A$) between 21.2 and 100 eV. The assignment of the photoelectron spectrum based on the analysis of intensity variations and width of vibrational peaks is consistent with the ion state orbital ordering $5e_1(1) < 7a_1(2) < 3e_2(3) < 4e_1(4)$ (band numbers are in parentheses) and is inconsistent with another recently proposed ordering $5e_1(1)$, $5e_1(2) < 7a_1$, $3e_2(3) < 4e_1(4)$, which takes the $5e_1$ vibronic effects into consideration. The experimental branching ratio results indicate a Ni 3p resonance effect around 75 eV in the photoionization process. The inner-valence spectrum has also been assigned with the aid of the Xα−SW calculations.

Introduction

CpNiNO is a fundamental, high-symmetry, half-sandwich organometallic molecule. The He I photoelectron spectrum (PES) of CpNiNO was first published in 1974.[1] The spectrum was assigned on the basis of SCF calculations.[2] Other more recent theoretical calculations using INDO[3] and MS−Xα methods[4] agreed with the original assignment: the first four bands were assigned $5e_1 < 7a_1 < 3e_2 < 4e_1$ in order of increasing binding energy (BE). However, recent variable-energy studies[5] on CpNiNO and Cp*NiNO, where Cp* is η^5-$CH_3C_5H_4$, have disputed this assignment. For example, the latest study suggests that the first two bands (separated by only ∼0.2 eV) could be due *just* to the $5e_1$ ionization split by vibrational effects from NO rather than by Jahn−Teller splitting.[5] The third band was then assigned to *both* the $7a_1$ and $3e_2$ ionizations.

In this study, we hoped to resolve the above controversy by carrying out a high-resolution variable-energy (21.2−100 eV) gas phase photoelectron study of CpNiNO using He I radiation and monochromatized synchrotron radiation. In addition, we have also performed an Xα−SW MO calculation and compared the observed relative band intensities (branching ratios, BR) with the theoretical branching ratios from both the Xα−SW calculations and the Gelius model treatment. This combined experimental−theoretical approach has been very successful in assigning the spectra of other organometallic molecules such as M(η^3-C_3H_5)$_2$ (M = Ni, Pd, Pt).[6]

Experimental Section

The compound was synthesized by the literature method.[7] The sample was purified by vacuum sublimation before recording the NMR, IR, and PES spectra. It was introduced into the gas cell of two photoelectron spectrometers by sublimation at 0 °C. The He I spectrum was obtained using an ESCA 36 spectrometer with a resolution of ∼20 meV.[8] The variable energy spectra from 21.2 to 100 eV were obtained at the Canadian Synchrotron Radiation Facility (CSRF) at the Aladdin storage ring using a modified ESCA 36 spectrometer fitted with a Quantar 36 position-sensitive detector.[9,10] The Grasshopper grazing incidence monochromator has been previously described.[11] The He I spectra were calibrated with the Ar $3p_{3/2}$ peak at 15.759 eV. For the synchrotron radiation spectra, the Xe 5s peak at 23.397 eV was used as the calibrant.

For the cross-section analyses, many of the spectra were fitted to Gaussian−Lorentzian line shapes using an iterative procedure.[12] Peak widths and shapes were basically constrained to obtain consistent fits from one photon energy to another. Experimental branching ratios (BR_i) were obtained using the resulting band areas (A_i) and the branching ratio formula, $BR_i = A_i/\sum A$.

Computational Details

Orbital energies and compositions of the NiCp fragment and CpNiNO molecule were calculated using the Xα−SW method as described earlier.[13] Geometrical data for these species were taken from the liturature.[14] Reported Xα−SW orbital energies

† The University of Western Ontario.
‡ Steacie Institute for Molecular Science.
§ Canadian Synchrotron Radiation Facility.
⊗ Abstract published in *Advance ACS Abstracts,* April 1, 1996.

(1) Evans, S.; Guest, M. F.; Hillier, I. H.; Orchard, A. F. *J. Chem. Soc., Faraday Trans. 2* **1974**, *70*, 417.
(2) Hillier, I. H.; Saunders, V. R. *Mol. Phys.* **1972**, *23*, 449.
(3) Böhm, M. C. *Z. Naturforsch.* **1981**, *36A*, 1361.
(4) Modelli, A.; Foffani, A.; Scagnolari, F.; Torroni, S,; Guerra, M.; Jones D. *J. Am. Chem. Soc.* **1989**, *111*, 6040.
(5) (a) Green, J. C.; Field, C.; Siggel, M. *Synchrotron Radiation: Appendix to the Daresbury Annual Report 1993/94*; Compiled by R. J. Cernik; The Daresbury Laboratory: Warrington, WA4 4AD, U.K., 1994; p 237. (b) Field, C. N.; Green, J. C.; Mayer, M.; Nasluzov, V. A.; Rösch, N.; Siggel, M. R. F. *Inorg. Chem.* **1996**, *35*, 2504.
(6) (a) Li, X.; Tse, J. S.; Bancroft, G. M.; Puddephatt, R. J.; Tan, K. H. *Organometallics* **1995**, *14*, 4513. (b) Hu, Y. F.; Bancroft, G. M.; Liu, Z. F.; Tan, K. H. *Inorg. Chem.* **1995**, *34*, 3716. (c) Li, X.; Bancroft, G. M.; Puddephatt, R. J.; Liu, Z. F.; Hu, Y. F.; Tan, K. H. *J. Am. Chem. Soc.* **1994**, *116*, 9543. (d) Yang, D. S.; Bancroft, G. M.; Puddephatt, R. J.; Tan, K. H.; Cutler, J. N.; Bozek, J. B. *Inorg. Chem.* **1990**, *29*, 4956.
(7) King, R. B. *Organometallic Syntheses*; Academic Press: New York and London, 1965; Vol. 1, p 169.
(8) Bancroft, G. M.; Bristow, D. J.; Coatsworth, L. L. *Chem. Phys. Lett.* **1981**, *82*, 344.
(9) Bozek, J. D.; Cutler, J. N.; Bancroft, G. M.; Coatsworth, L. L.; Tan, K. H.; Yang, D. S. *Chem. Phys. Lett.* **1990**, *165*, 1.
(10) Liu, Z. F.; Coatsworth, L. L.; Tan, K. H. *Chem. Phys. Lett.* **1993**, *203*, 337.
(11) (a) Tan, K. H.; Bancroft, G. M.; Coatsworth, L. L.; Yates, B. W. *Can. J. Phys.* **1982**, *60*, 131. (b) Bancroft, G. M.; Bozek, J. D.; Tan, K. H. *Phys. Can.* **1987**, 113.
(12) Bancroft, G. M.; Adams, J.; Coatsworth, L. L.; Bennewitx, C. D.; Brown, J. D.; Westwood, W. D. *Anal. Chem.* **1975**, *47*, 586.

0020-1669/96/1335-2515$12.00/0

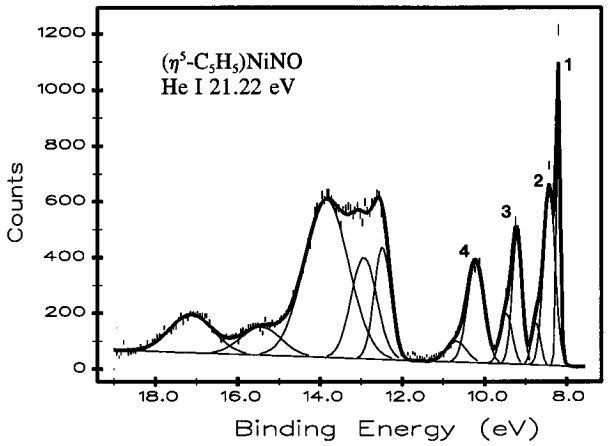

Figure 1. Broad-range He I spectrum of CpNiNO.

of NO were used.[15] C_{5v} symmetry was assumed for NiCp and CpNiNO with the *z* axis along the C_5 axis and with Ni located at the origin.

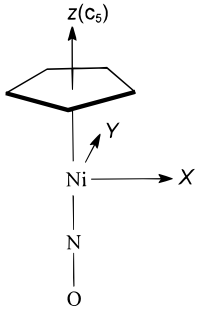

The exchange α parameters used in each atomic region were taken from Schwarz's tabulation,[16] except those of hydrogen, for which 0.777 25 was used. Overlapping atomic sphere radii were used with the outer-sphere radius tangential to the outermost atomic spheres. An l_{max} of 4 was used around the outer-sphere region, whereas l_{max} values of 3, 1, and 0 were used around Ni, C, and H atoms, respectively. Photoionization cross sections (σ) were calculated for the outer-valence levels of CpNiNO, using the Xα−SW cross-section program of Davenport.[17] The calculations were performed with the converged Xα−SW transition state potential for the highest occupied molecular orbital (HOMO), modified with a Latter tail to correct for large *r* behavior. In addition to the parameters used in the Xα−SW calculations on molecular orbitals (MO), the maximum azimuthal quantum number, l_{max}, for final states was extended to 8, 4, 2, and 1 around the outer sphere, nickel, carbon, and hydrogen regions, respectively. In the calculation of transition state potential, half of an electron is removed from the HOMO of molecular orbitals. All symmetry-allowed photoionization processes based on the dipolar selection rule were included in the calculations.

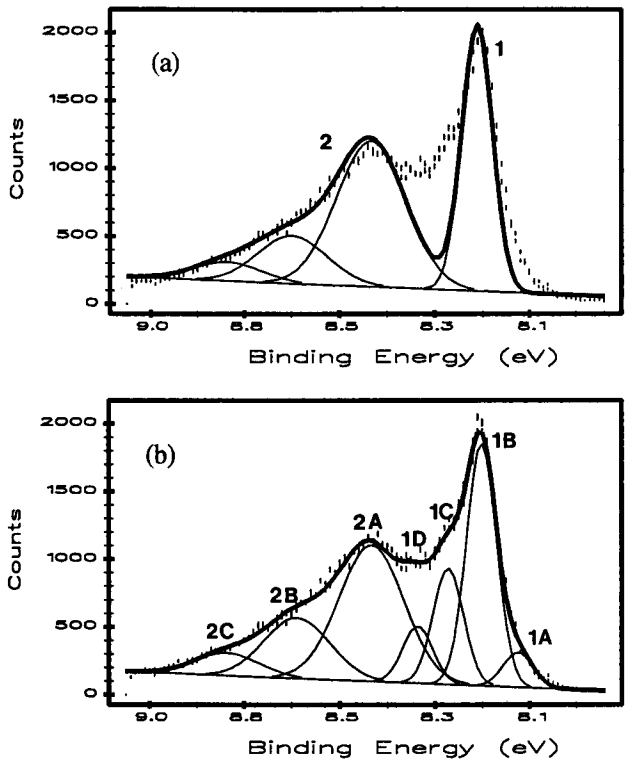

Figure 2. He I close up spectrum for the first two bands of CpNiNO.

Results

(a) The Photoelectron Spectra. A broad-range He I photoelectron spectrum from 7.5 to 19 eV binding energy is shown in Figure 1. This spectrum is essentially the same as previously reported.[1,5] To view bands 1 and 2 in more detail at high resolution, we show a high-quality spectrum of just these bands in Figure 2. There is clearly some vibrational structure on both bands. For example, a fit with no vibrational structure on band 1 gives a poor fit (Figure 2a). We have, therefore, fit two vibrational series to this spectrum with fixed vibrational energies (70 meV for band 1, 150 meV for band 2) and fixed line width (75 meV for band 1, 160 meV for band 2). The vibrational energies are tentatively assigned to the two vibrational modes,[18] E_2 (ring distortion) and A_1 (ring breathing), which have vibrational frequencies of 565 and 1112 cm^{-1}. It is important to note that, although this is not a unique fit, the line widths of the peak or peaks in band 2 (defined mostly by peak 2A) are obviously much larger than the narrow line width of band 1 (defined by peak 1B on the low-BE side of band 1).

A spectrum taken at 35 eV photon energy compared to the 21.2 eV spectrum (Figure 3) shows another important effect: the relative intensity of band 2 increases greatly from 21.2 to 35 eV. Figure 3 also shows that the intensities of bands 3 and 4 also increase dramatically from 21.2 to 35 eV. Other representative spectra of the first four bands are shown in Figure 4 at 50, 75, 90, and 100 eV. Relative band intensity variations are immediately obvious. In particular, the intensity of band 3 increases greatly at higher photon energies.

(b) Electronic Structure of Ni(η^5-C_5H_5)NO. The Xα−SW orbital energies and compositions for the NiCp fragment are listed and plotted in Table 1 and Figure 5, respectively. The electron configuration is $(core)(3a_1)^2(5e_1)^4(1e_2)^4(4a_1)^2(6e_1)^3$. There are three types of orbital interactions (π, σ, and δ) for NiCp.[19] Among them, $4a_1$ and $3a_1$ are the σ type orbitals which are mainly nonbonding for NiCp. Because the Cp π orbital in

(13) (a) Yang, D. S.; Bancroft, G. M.; Puddephatt, R. J.; Bozek, J. D.; Tse, J. S. *Inorg. Chem.* **1989**, *28*, 1. (b) Yang, D. S.; Bancroft, G. M.; Puddephatt, R. J.; Bursten, B. E.; McKee, S. D. *Inorg. Chem.* **1989**, *28*, 872. (c) Yang, D. S.; Bancroft, G. M.; Puddephatt, R. J. *Inorg. Chem.* **1990**, *29*, 2118. (d) Yang, D. S.; Bancroft, G. M.; Dignard-Bailey, L.; Puddephatt, R. J.; Tse, J. S. *Inorg. Chem.* **1990**, *29*, 2487. (e) Yang, D. S.; Bancroft, G. M.; Puddephatt, R. J.; Tse, J. S. *Inorg. Chem.* **1990**, *29*, 2496.
(14) Jolly, P. W. In *Comprehensive Organometallic Chemistry*; Wilkinson, G., Ed.; Pergamon Press: London, 1982; Vol. 6, p 210.
(15) Salahub, D. R.; Messmer, R. P. *J. Chem. Phys.* **1976**, *64*, 2039.
(16) (a) Schwarz, K. *Phys. Rev. B* **1972**, *5*, 2466. (b) Schwarz, K. *Theor. Chim. Acta* **1974**, *34*, 225.
(17) (a) Davenport, J. W. Ph.D. Dissertation, University of Pennsylvania, 1976. (b) Davenport, J. W. *Phys. Rev. Lett.* **1976**, *36*, 945.
(18) Paliani, G.; Cataliotti, R.; Poletti, A.; Foffani, A. *J. Chem. Soc., Dalton Trans.* **1972**, 1741.

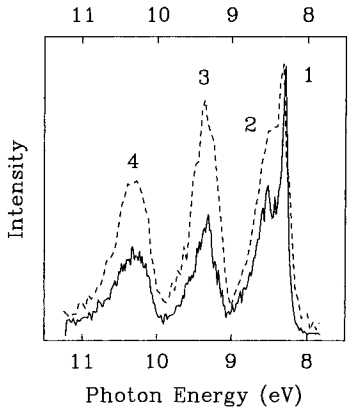

Figure 3. Photoelectron spectra of CpNiNO recorded at He I photon energy (21.2 eV, solid line) and at 35 eV photon energy (dashed line). Both of the spectra are normalized to the height of band 1.

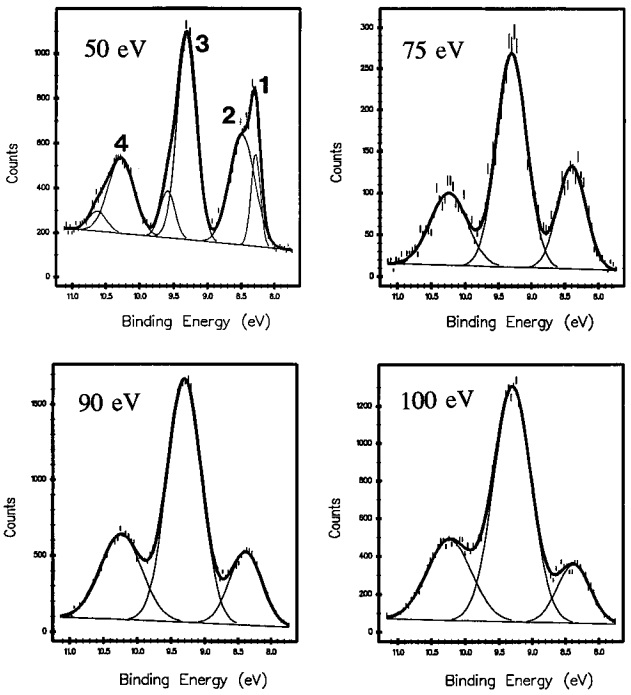

Figure 4. Representative variable-energy spectra for the first four bands of CpNiNO at 50, 75, 90, and 100 eV photon energy.

Table 1. Xα−SW MO Energies and Compositions (%) for the NiCp Fragment

orbital	energy (eV)	Ni 4p	Ni 4s	Ni 3d	C 2p	C 2s	inter	outer
$6e_1$	−3.35	4.9		63.6	31.3		20.5	4.7
$4a_1$	−4.64		1.4	97.5	0.5		7.0	0.7
$1e_2$	−4.82			98.0	2.7		6.4	0.5
$5e_1$	−5.78	1.3		53.6	44.4	0.5	18.6	0.7
$3a_1$	−8.82	2.3	11.1	0.7	85.6	0.2	30.7	1.1

a_1 symmetry points toward the nodal cone of the metal $3d_{z^2}$ orbital,[20] it can only interact a small amount with the high-lying Ni 4s orbital to form the $3a_1$ molecular orbital (MO), thus leaving $4a_1$ essentially of Ni $3d_{z^2}$ character. The $1e_2$ MO is of δ type, which has predominant Ni $3d_{x^2-y^2}/3d_{xy}$ character. These electrons remain mainly nonbonding because the *xy* plane is parallel with the Cp plane. Thus, the δ type overlap with the Cp π orbitals is not very large. The $6e_1$ and $5e_1$ MO's involve π type interactions. They contain approximately half Ni $3d_{xz}/3d_{yz}$ composition, indicating the former is the antibonding (out-of-phase) and the latter is the bonding (in-phase) interaction of Ni $3d_{xz}/3d_{yz}$ with the Cp e_1 orbitals. The antibonding orbitals, the $6e_1$ set, are not fully filled with electrons. Thus these π type interactions contribute to the bond order. The MCp fragment orbitals have been illustrated in the literature.[21] The orbital ordering from our calculation is in agreement with the earlier result.

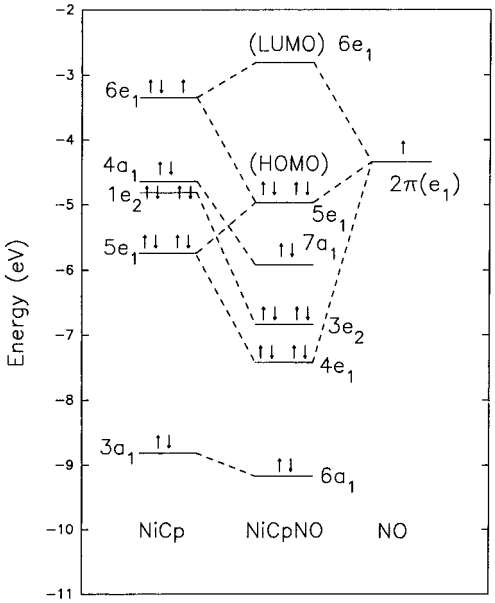

Figure 5. Molecular orbital diagram of NiCp, CpNiNO, and NO calculated by the Xα−SW method. Dashed lines show the orbital interaction correlations. The calculated energies for other occupied NO orbitals are lower than −11 eV, so they are not involved.

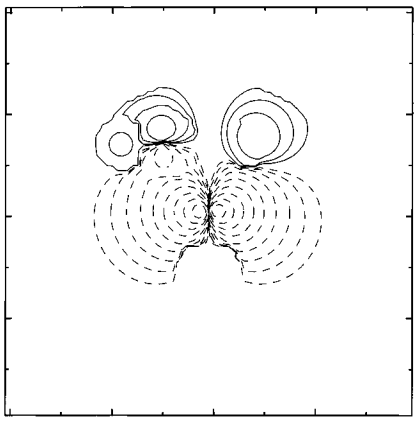

Figure 6. Xα−SW MO contour map of the CpNiNO $3e_2$ orbital. It clearly shows that NO does not have orbitals in e_2 symmetry to overlap with the $3d_{x^2-y^2}/3d_{xy}$ orbitals and that Cp π orbitals in e_2 symmetry overlap very little with the Ni 3d.

The Xα−SW MO compositions and energies for valence molecular orbitals of CpNiNO are listed and plotted in Table 2 and Figure 5, respectively. Its electron configuration is

$$(\text{core})(6a_1)^2(4e_1)^4(3e_2)^4(7a_1)^2(5e_1, \text{HOMO})^4(6e_1, \text{LUMO})^0$$

The reported Xα−SW MO energy of nitrogen monoxide $(2\pi)^1$ is also shown in Figure 5.[15] The classification of three types of orbital interactions (π, σ, and δ) is still suitable for CpNiNO. The δ type MO ($3e_2$) retains its nonbonding Ni $3d_{x^2-y^2}/3d_{xy}$ character since these d orbitals cannot properly overlap with

(19) Elschenbroich, C.; Salzer, A. *Organometallics: A Concise Introduction*, 2nd ed.; VCH Publishers Inc.: New York, 1992; pp 318−319.
(20) Mingos, D. M. P. In *Comprehensive Organometallic Chemistry*; Wilkinson, G., Ed.; Pergamon Press: London, 1982; Vol. 3, p 28.
(21) Albright, T. A.; Burdett, J. K.; Whangbo, M.-H. *Orbital Interactions in Chemistry*; John Wiley & Sons: New York, 1985; pp 387−388.

Table 2. Xα−SW MO Energies and Compositions (%) for NiCpNO

orbital	energy (eV)	Ni 4p	Ni 4s	Ni 3d	C 2p	C 2s	N 2p	N 2s	O 2p	O 2s	H 1s	inter	outer
					Outer Valence								
$6e_1$ (LUMO)	−2.81			33.0	17.0	0.2	33.4		16.4			15.7	0.8
$5e_1$ (HOMO)	−4.97	8.1		2.4	55.3		16.5		17.6			31.4	0.8
$7a_1$	−5.92	2.1	7.5	85.7	1.5		0.8	1.0	2.1		0.5	13.4	0.1
$3e_2$	−6.85			98.5	1.3							4.8	
$4e_1$	−7.43			71.7	14.9	0.6	2.2		10.1		0.4	9.0	0.2
$6a_1$	−9.17	4.5	7.9		86.7	0.3	0.3	0.3				27.3	0.7
					Inner Valence								
$2e_2$	−11.13			0.2	78.5	0.9					20.4		0.3
$3e_1$	−11.86	0.2		1.2	63.6	0.9	0.4		1.3		32.3		0.5
$2e_1$	−12.75	0.4		4.4	1.3		37.4		55.7		0.8	15.0	0.1
$5a_1$	−15.20	0.6		0.2	55.4	3.6	0.2	0.1	0.2		39.7		0.5
$1e_2$	−15.45			0.3	38.9	32.6					28.3		0.3
$4a_1$	−17.31	3.1	2.4	5.7	0.1	0.2	23.8	0.4	44.4	19.8	0.2		0.7
$1e_1$	−19.45	0.4		0.9	16.1	69.3					13.3		0.1
$3a_1$	−20.18	9.0	5.9	11.5		0.9	15.7	39.4	3.5	14.0	0.1		0.1
$2a_1$	−24.03	0.7	1.8	1.0	17.1	77.1	0.2	0.3			1.9		
$1a_1$	−36.82						20.9	23.1	19.9		36.2		

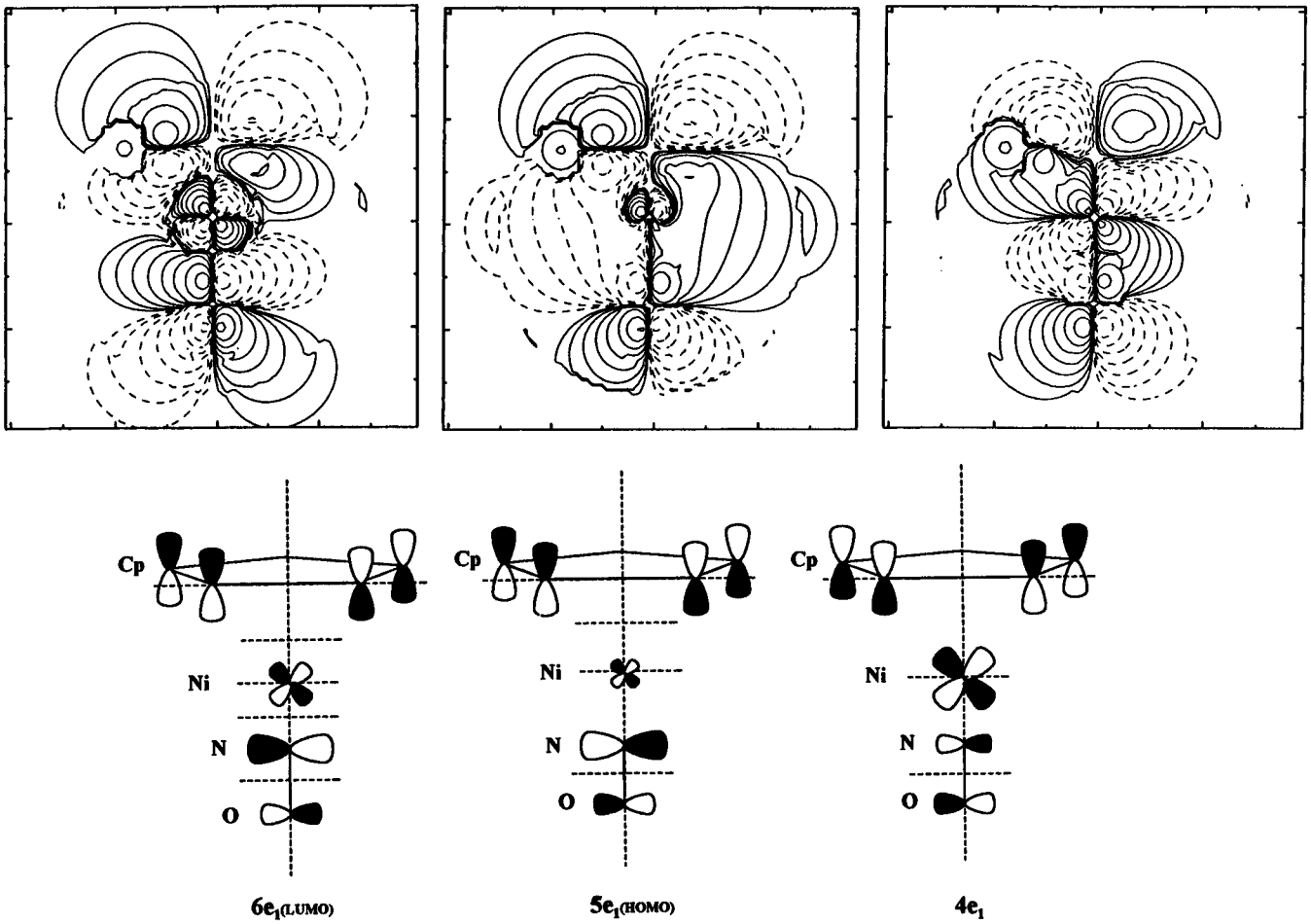

Figure 7. Xα−SW MO contour maps of $6e_1$ (LUMO), $5e_1$ (HOMO), and $4e_1$ for CpNiNO. The schematic contour diagrams are plotted below. The dashed lines in them represent the nodal plane.

NO orbitals (no e_2 orbital exists for NO). The contour map for one of the doubly-degenerate $3e_2$ MO's is shown in Figure 6. The π type MO's in CpNiNO still make the main contribution to bonding. The σ type MO of $7a_1$ has mainly NiCp $4a_1$ character. However, it has some degree of interaction with NO 3σ and 2σ MO's. The $6a_1$ MO has mainly Cp π_1 orbital character.

Compared with the NiCp fragment, the number of π type MO's in the outer valence of CpNiNO is increased by one set due to the participation of NO 2π MO's which have e_1 symmetry. The symmetry and energy of NO 2π orbitals match those of NiCp $6e_1$ and $5e_1$. The MO compositions in Table 2 show that $5e_1$ and $4e_1$ of CpNiNO have a considerable amount of 2p character of nitrogen, oxygen, and carbon, suggesting that they are formed by interaction of the NO 2π orbital with both NiCp $6e_1$ and $5e_1$ orbitals (a three-center-orbital interaction). For the NO 2π set, one orbital is singly occupied and the other is empty. The NiCp $6e_1$ set has a singly and a doubly occupied orbital. Therefore the π type three-center orbital interaction makes a major contribution to the bond order of the molecule. The MO composition of the lowest unoccupied molecular orbital ($6e_1$, LUMO) shows a considerable amount of NO and Ni 3d contribution, suggesting that it is the empty set formed by the three-center orbital interaction.

In order to confirm the existence of the three-center orbital interaction, we draw the *xz*-plane contour maps for the resultant $6e_1$ (LUMO), $5e_1$ (HOMO), and $4e_1$ MO's in CpNiNO (Figure

7). This figure indicates that the NO 2π orbital is involved in all the three MO's. These contour maps show the following interacting patterns among Cp(π), Ni(3d), and NO(2π):

$$6e_1: \quad \pi Cp(e_1) - Ni(d_{xz} \text{ or } d_{yz}) - NO(2\pi)$$

$$5e_1: \quad \pi Cp(e_1) - Ni(d_{xz} \text{ or } d_{yz}) - NO(2\pi)$$

$$4e_1: \quad \pi Cp(e_1) - Ni(d_{xz} \text{ or } d_{yz}) - NO(2\pi)$$

Also, the numbers of nodal planes are 6 for $6e_1$, 5 for $5e_1$, and 4 for $4e_1$ (Figure 7). The above features of orbital composition, contour distribution, nodal plane number, and net bond order can be explained by the three-center orbital interaction. In fact, for the structure of CpNiNO, whether the molecule takes a three-center or a two-center orbital interaction in formation of the bonding depends on how close the energy of the NO 2π is to that of the NiCp $5e_1$. If their energies are not close enough, the NO 2π orbital would have little involvement in the $4e_1$ MO of CpNiNO, and we could assume that the valence orbital interaction between NiCp and NO was mainly a regular two-center interaction (between $6e_1$ of NiCp and 2π of NO), which formed one antibonding MO (LUMO, $6e_1$) and one bonding MO (HOMO, $5e_1$) for CpNiNO, leaving the $4e_1$ of CpNiNO as a nonbonding MO from NiCp. However, the Xα−SW calculation shows a 2.2% N 2p and a 10.1% O 2p composition for the $4e_1$ MO of CpNiNO (Table 2). Therefore, the involvement of a three-center orbital interaction has to be considered. A similar account of the three-center mode has been reported for the bonding between metal d and CO 1π and 2π orbitals.[22]

There is also a σ type three-center orbital interaction among NiCp $4a_1$, NO 3σ, and NO 2σ orbitals to form three CpNiNO MO's ($7a_1$, $4a_1$, and $3a_1$), which will be discussed later. Since these three MO's are all fully filled, the σ type three center interaction does not make a net contribution to the bond order.

(c) Theoretical Photoelectron Branching Ratios. For CpNiNO, we obtained theoretical cross sections using both the Gelius[23] and Xα method and then obtained branching ratios ($BR_i = \sigma_i/\sum\sigma_i$, where σ_i are the calculated cross sections) to compare with the experimental BR_i values. In the Gelius treatment, the cross section of an individual MO is assumed to be proportional to the sum of the atomic cross sections (σ_{A_j}) of its components weighted by the "probability" $(P_{A_j})_i$ of finding in the ith molecular orbital an electron belonging to the atomic orbital A_j:

$$\sigma_i \propto \sum_j (P_{A_j})_i \sigma_{A_j}$$

where $(P_{A_j})_i$ is given approximately by the orbital composition from our Xα calculations and σ_{A_j} are the theoretical atomic cross sections as a function of photon energy. In this work, Yeh and Lindau's data,[24] obtained by the Hartree−Slater central field method, were used. A qualitative guide to the variations in molecular cross sections and branching ratios can be obtained by looking at the atomic cross sections in Figure 8a. Thus the Ni 3d orbitals show an increase in cross section above threshold, before decreasing in markedly different ways at higher energies. In contrast, the C 2p, N 2p, and O 2p orbitals show a monotonic decrease in cross section over the whole range. This is reflected in the cross-section and branching ratio changes. The branching ratio method is a relative band intensity method. It can be visualized by the ratio of photoionization cross sections between the Ni 3d and 2p of C, N, and O atomic subshells (Figure 8b). The latter cross sections represent the main composition of ligand-based MO's for the title compound. These ratios in Figure 8b show that the relative intensity of Ni 3d based bands increase and that of ligand-based bands decrease with the increase of photon energy.

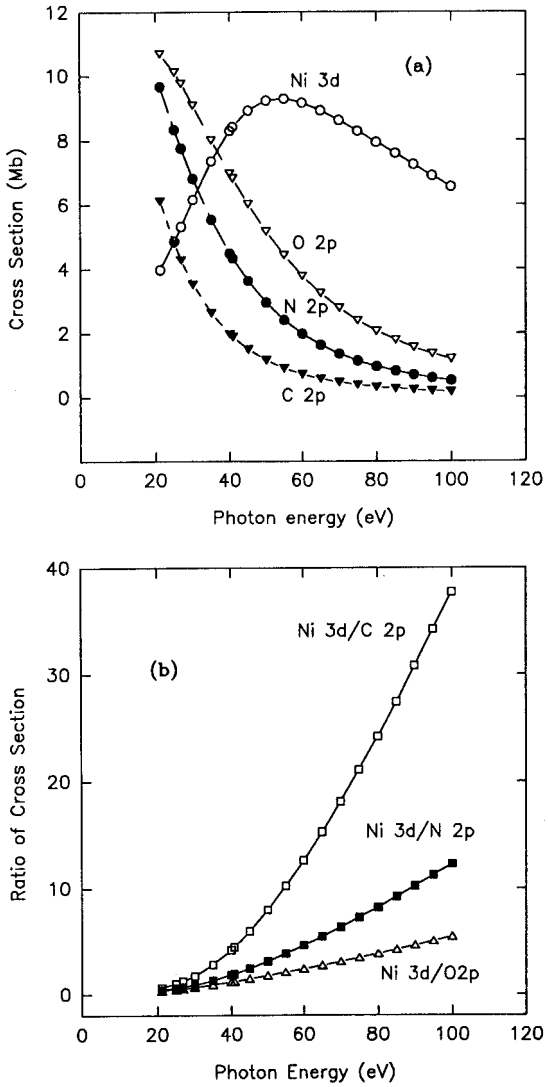

Figure 8. (a) Photoionization cross sections calculated by Yeh and Lindau[22] for atomic subshells of Ni 3d, O 2p, N 2p, and C 2p. (b) Ratio of photoionization cross sections between Ni 3d and a ligand orbital component, C 2p.

Discussion

(a) Assignment of the First Four Bands. Our assignment is based mainly on the high-resolution He I spectrum of bands 1 and 2 (Figure 2) and the comparison of experimental and theoretical branching ratio trends from 21.2 to 100 eV for bands 1+2, 3, and 4 (Figures 9 and 10). Since there is a Ni 3p resonance effect which influences the intensities above 75 eV and is not included in the calculations, we begin by discussing the intensities and branching ratios below 75 eV.

It is generally agreed that the first four bands arise from the four outermost MO's ($5e_1$, $7a_1$, $3e_2$, and $4e_1$). Is there a direct one to one correspondence of the four bands to the four MO's,[1−4] or do bands 1 and 2 arise just from the vibrationally

(22) (a) Mingos, D. M. P In *Comprehensive Organometallic Chemistry*; Wilkinson, G., Ed.; Pergamon Press: London, 1982; Vol. 3, p 2−5. (b) Johnson, J. B.; Klemperer, W. G. *J. Am. Chem. Soc.* **1977**, *99*, 7132.

(23) (a) Gelius, U. In *Electron Spectroscopy*; Shirley, D. A., Ed.; North Holland: Amsterdam, 1972; p 311. (b) Bancroft, G. M.; Malmquist, P.-Å; Svensson, S.; Bailier, E.; Gelius, U.; Siegbahn, K. *Inorg. Chem.* **1978**, *17*, 1595.

(24) Yeh, J. J.; Lindau, I. *At. Nucl. Data Tables* **1985**, *32*, 1.

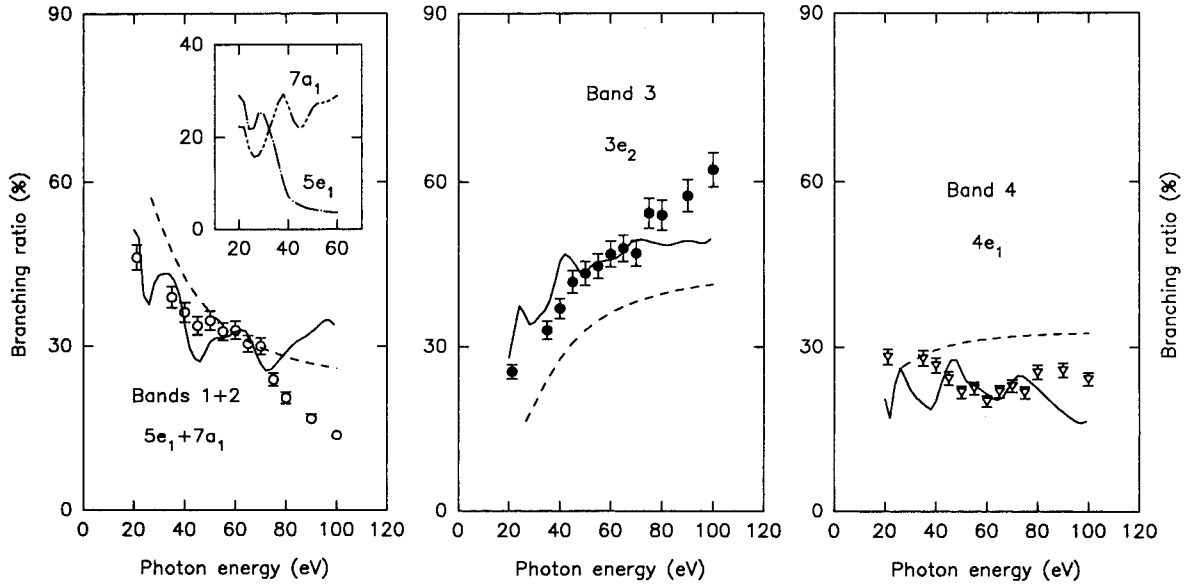

Figure 9. Branching ratio comparison between experimental values (symbols) and values calculated with the Xα method (solid line) and the Gelius model treatment (dashed line) for assignment I. Individual Xα−SW branching ratios for bands 1 and 2 are also shown in the inserted figure.

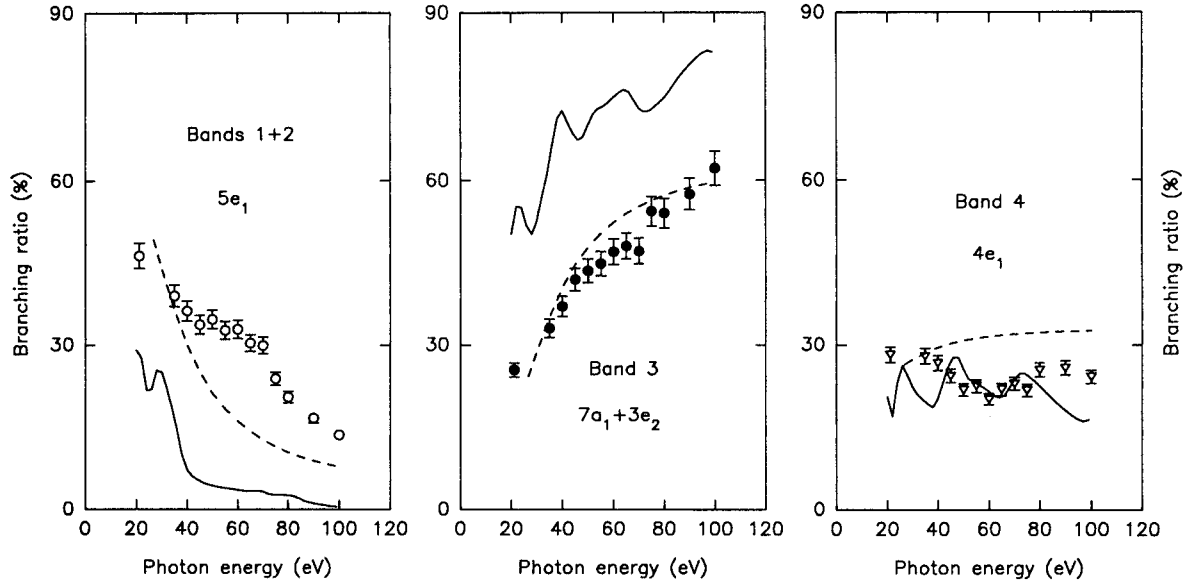

Figure 10. Branching ratio comparison between experimental values (symbols) and values calculated with the Xα method (solid line) and the Gelius model treatment (dashed line) for assignment II.

split $5e_1$ MO, with band 3 arising from the $7a_1$ and $3e_2$ MO's?[5] Unfortunately, because bands 1 and 2 are only separated by 0.22 eV and have complex vibrational structure, it is not possible to estimate accurately the BR for bands 1 and 2 separately. It is obvious from Figures 2a, 3, and 4a that a one-peak fit to band 1 cannot give satisfactory individual band areas. If the width of peak 1 is constrained to the He I single peak width from Figure 2a of 75 meV, it is obvious that the width and area of band 1 are dramatically underestimated in this fit (in Figure 4a, however, such a fit certainly gives the overall area of bands 1+2 accurately). Despite this problem of separating out bands 1 and 2, Figure 3 shows conclusively that the area of band 2 increases greatly from 21.2 to 35 eV.

Already then, we have strong qualitative evidence that bands 1 and 2 do not arise primarily from the same orbital, vibrationally split by the NO stretching frequency of ~0.22 eV.[5] First, the increase in intensity of band 2 (and bands 3 and 4) from 21.2 to 35 eV (Figure 3) strongly indicates that band 2 (and bands 3 and 4) arises from an orbital having high Ni 3d character. Second, the very different widths of bands 1 and 2 (and their component peaks) strongly suggest that these two bands originate from *different* MO's.

The experimental branching ratios provide more evidence for the validity of the original assignment. It is important to note that our experimental branching ratios in Figure 9 are in excellent agreement over the whole energy range with those published recently.[5] This experimental agreement is important because the spectra were taken with very different types of photoelectron spectrometers.

From Figure 8, we know that the intensity of a Ni 3d based band should increase and that of a ligand-based band should decrease from low to high photon energy; and a band corresponding to an MO with intermediate Ni 3d or ligand C/N/O 2p composition should behave in an intermediate way. From 21.2 to 75 eV, the experimental branching ratio (BR) of band 3 increases (Figure 9 or 10). So, the $3e_2$ MO with 98.5% Ni 3d composition calculated by the Xα−SW method (Table 2) must be assigned to this ionization. The BR plot for band 4 is quite constant (Figure 9 or 10), and this behavior is consistent with the assignment of this band to the $4e_1$ MO with 71.7% Ni

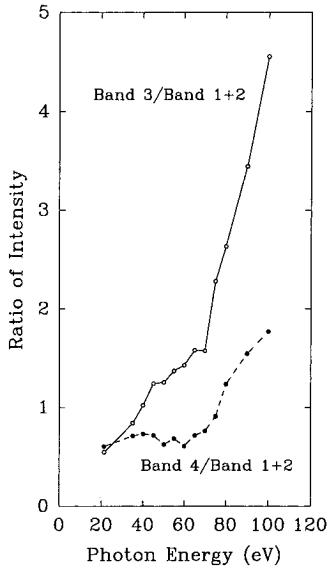

Figure 11. Ratio of band intensities of band 3 and band 4 to bands 1+2.

Table 3. Ground-State Xα Energies (*E*), Experimental Ionization Potentials (IP), Xα Ni 3d Compositions, and Relaxation Energies (Δ = −E − IP) for NiCpNO

orbital	*E* (eV)[a]	IP (eV)[a]	Xα Ni 3d compn (%)[a]	Δ (eV)[a]
		Assignment I		
$5e_1$	0.00	0.00	0.0	0.00
$7a_1$	−0.95	0.19	83.3	0.76
$3e_2$	−1.88	1.01	96.1	0.87
$4e_1$	−2.46	1.98	69.3	0.48
		Assignment II		
$5e_1$	0.00	0.00	0.0	0.00
$7a_1$	−0.95	1.01	83.3	−0.09
$3e_2$	−1.88	1.01	96.1	0.87
$4e_1$	−2.46	1.98	69.3	0.48

[a] Values are normalized to the $5e_1$ MO.

3d character. The branching ratio of bands 1+2 decreases. Obviously these two bands must contain the $5e_1$ orbital with only 2.4% Ni 3d character. Combined with the evidence from Figures 2 and 3 discussed above, these qualitative arguments strongly indicate that the IP ordering is

$$5e_1(1) < 7a_1(2) < 3e_2(3) < 4e_1(4) \quad \text{(assignment I)}^{1-4}$$

and not

$$5e_1(1) < 5e_1(2) < 7a_1 = 3e_2(3) < 4e_1(4) \quad \text{(assignment II)}^{5}$$

The detailed comparison of experimental and theoretical branching ratios gives further evidence that assignment I (Figure 9) gives better agreement between theory and experiment than assignment II (Figure 10). Although there is not as good agreement between the Gelius and Xα−SW cross sections as is usual,[6] it is immediately obvious that if bands 1+2 were *just* from the $5e_1$ orbital, the experimental branching ratio is dramatically higher than both theoretical cross sections between 40 and 75 eV. Certainly, there is far better agreement between theory and experiment up to 75 eV if bands 1 and 2 are assigned to *both* the $5e_1$ and $7a_1$ orbital ionizations.

Finally, it is important to note that our assignment does not rule out that part of the intensity in peak 2A arises from the NO vibrational effect on peak 1B. However, our analysis strongly suggests that this effect is not a *major* contributing factor to peak 2A.

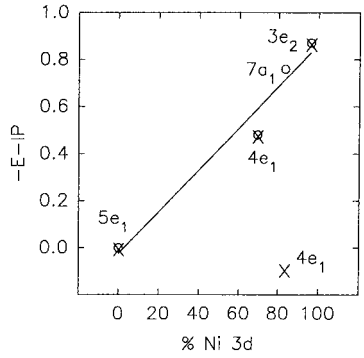

Figure 12. Correlations between relaxation energies (−E − IP, where *E* is the Xα eigenvalue in the ground state and IP is the experimental ionization potential) and Xα Ni 3d compositions for $5e_1$, $7a_1$, $3e_2$, and $4e_1$ MO's of CpNiNO. All values are normalized to those of the $5e_1$ MO (○, assignment I; ×, assignment II).

(b) Ni 3p Resonance Effect. Near the Ni 3p ionization threshold at ∼75 eV in many Ni compounds (the BE's for the $3p_{3/2}$ and $3p_{1/2}$ levels of the Ni atom are 73 and 75 eV, respectively[25]), the Ni 3d cross section is enhanced by the 3p → 3d giant resonance absorption.[26] The 3p → 3d resonant absorption process for CpNiNO may be represented by[5]

$$3p^6(4e_1)^4(3e_2)^4(7a_1)^2(5e_1)^4(6e_1)^0 \rightarrow 3p^5(4e_1)^4(3e_2)^4(7a_1)^2(5e_1)^4(6e_1)^1$$

where the $6e_1$ orbital has substantial Ni 3d character (Table 2).

After Super Coster Kronig (SCK) decay, the final state can be the same as that from direct photoionization of a valence electron, such as the $3e_2$ electron:

$$3p^5(4e_1)^4(3e_2)^4(7a_1)^2(5e_1)^4(6e_1)^1 \rightarrow 3p^6(4e_1)^4(3e_2)^3(7a_1)^2(5e_1)^4(6e_1)^0 + e$$

This process leads to the increase in BR seen above 75 eV for the orbitals having high Ni 3d character (the $3e_2$, $4e_1$, and $7a_1$ orbitals) with a concomitant decrease in the $5e_1$ BR. The involvement of the ligand-based $5e_1$ MO (2.4% Ni 3d character, Table 2) causes the combined BR of bands 1+2 to decrease above 75 eV (Figure 9 or 10).

The Ni 3p resonance effect is perhaps best seen in Figure 11, where we plot the intensity ratios of band 4 and band 3 divided by the intensity of bands 1+2. Note that, as expected, there is a dramatic increase in these ratios above ∼70 eV; and the largest increase arises from the band 3 plot due to the highest Ni 3d character of the $3e_2$ orbital (Table 2). Moreover, the band 4/bands 1+2 ratios below 75 eV of <1 provide further evidence that assignment I is correct. Band 4 arises from the $4e_1$ orbital of 71.7% Ni 3d character. If bands 1+2 arise from the $5e_1$ MO of 2.4% Ni 3d character, the ratio of band 4/bands 1+2 in Figure 11 should increase greatly from 20 to 75 eV. Instead, this ratio remains approximately constant because band 2 arises from the $7a_1$ orbital of high Ni 3d character. To restate, the ratio remains constant because of the large increase in intensity of band 2 from 21.2 to 75 eV due to the high Ni 3d character of the $7a_1$ orbital.

(25) Briggs, D., Ed. *Handbook of X-ray and Ultraviolet Photoelectron Spectroscopy*; Heyden: London, 1977.
(26) (a) Brennan, J.; Cooper, G.; Green, J. C.; Payne, M. P.; Redfern, C. M. *J. Electron Spectrosc. Relat. Phenom.* **1993**, *66*, 101. (b) Brennan, J. G.; Green, J. C.; Redfern, C. M.; MacDonald, M. A. *J. Chem. Soc., Dalton Trans.* **1990**, 1907.

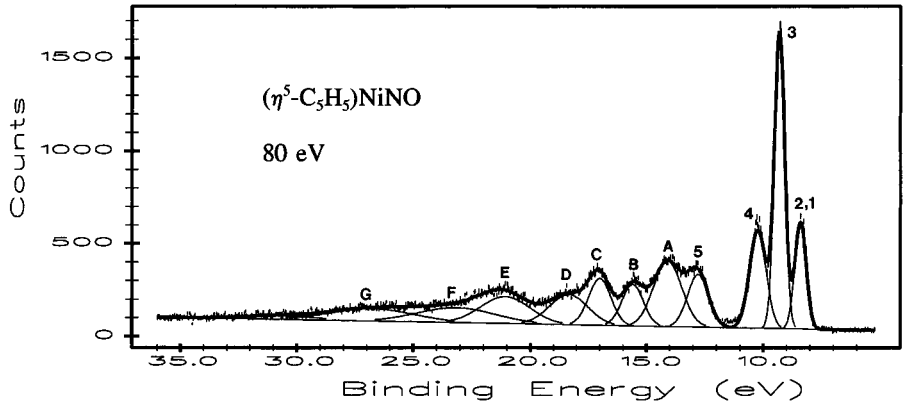

Figure 13. Broad-range photoelectron spectrum of CpNiNO at 80 eV photon energy.

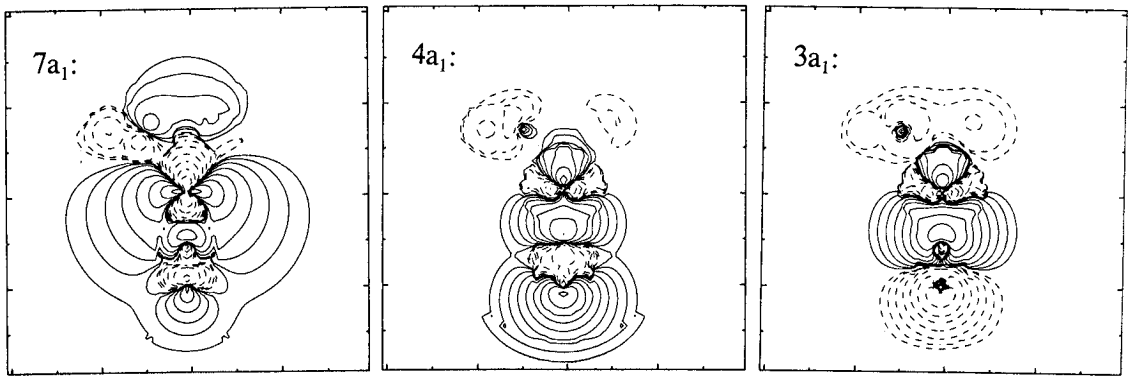

Figure 14. Xα−SW MO contour maps for $7a_1$, $4a_1$, and $3a_1$ of CpNiNO.

It should also be noted that the Ni 3p resonance effect causes poorer agreement between theoretical and experimental branching ratios for bands 1+2 and band 3 above 75 eV (Figure 9).

(c) Relaxation Energies. It is generally recognized that, for transition metal complexes,[1,27] "greater orbital relaxation is associated with the localized metal orbitals than with the relatively delocalized ligand MO's". It is perhaps interesting to note that the sequence of orbital relaxation energies, using assignment I, indeed correlates well with the magnitude of the Ni 3d orbital composition (Table 3, Figure 12).

Our Xα−MO compositions show that, among the four valence MO's ($5e_1$, $7a_1$, $3e_2$, $4e_1$), only the $5e_1$ orbital has very low Ni 3d composition (2.4% Ni 3d) and has mainly ligand character. All others have predominant Ni 3d composition (>71.7% Ni 3d). So, the $7a_1$, $3e_2$, and $4e_1$ orbitals should show larger relaxation upon ionization relative to the $5e_1$ MO. The ionization potentials (IP) of $7a_1$, $3e_2$, and $4e_1$ should shift toward the value of the $5e_1$ MO from their Koopmans' ionization potentials (=−*E*, where *E* is the ground-state energy which is calculated with the Xα method). In this paper, we term the shift for these MO's as "−E − IP", the "relaxation energies" relative to $5e_1$, where IP is the experimental ionization potential. The $5e_1$ MO is the reference for us to make the study. Its relaxation energy and Ni 3d composition are arbitrarily set to zero due to its greatest ligand-based orbital character, and its Xα ground-state energy (*E*) and ionization potential (IP) are also set to zero for simplicity (Table 3). Thus, for assignment I, the "relaxation energies" of $7a_1$, $3e_2$, and $4e_1$ are found to be well correlated with the Xα Ni 3d compositions relative to $5e_1$ (Table 3 and Figure 12). However, for assignment II (Figure 12), the $7a_1$ lies far off the correlation, not consistent with the high Ni 3d character for this orbital.

(27) Green, J. C. *Struct. Bonding* **1981**, *43*, 37.

Table 4. Assignment of the Photoelectron Spectrum of NiCpNO

orbital	energy (eV)	IP (eV)	assignment	main character
		Outer Valence		
$5e_1$	−4.97	8.29	1	Cp π and NO 2π
$7a_1$	−5.92	8.48	2	Ni 3d
$3e_2$	−6.85	9.30	3	Ni 3d
$4e_1$	−7.43	10.27	4	Ni 3d, Cp π and NO 2π
$6a_1$	−9.17	12.64	5	Cp π
		Inner Valence		
$2e_2$	−11.13	14.1	A	Cp σ
$3e_1$	−11.86	15.6	B	Cp σ
$2e_1$	−12.75	17.0	C	NO 1π
$5a_1$	−15.20	18.3	D	Cp σ
$1e_2$	−15.45	18.3	D	Cp σ
$4a_1$	−17.31	18.3	D	NO 3σ
$1e_1$	−19.45	21.1	E	Cp σ
$3a_1$	−20.18	21.1	E	NO 2σ
		23.2	F	NO shake-up
$2a_1$	−24.03	26.8	G	Cp σ
$1a_1$	−36.82	out of range		NO 1σ

(d) Inner-Valence Spectra. A broad-range photoelectron spectrum of CpNiNO out to 35 eV BE is shown in Figure 13. This spectrum displays the four bands shown earlier (Figure 1), and a number of other bands (labeled A−G) which are arbitrarily termed the inner-valence region. The MO compositions and energies of these orbitals are shown in Table 2. They can be grouped into mainly Cp orbitals and NO orbitals. The Cp σ orbitals are $2e_2$, $3e_1$, $5a_1$, $1e_2$, $1e_1$, and $2a_1$. The NO orbitals are $2e_1$ (NO 1π), $4a_1$ (NO 3σ), $3a_1$ (NO 2σ), and $1a_1$ (NO 1σ). The $4a_1$ (NO 3σ) and $3a_1$ (NO 2σ) orbitals show 5.7% and 11.5% Ni 3d character, respectively, suggesting that Ni $3d_{z^2}$ overlaps with NO 3σ and 2σ simultaneously through a σ type three-center orbital interaction to form three MO's, $7a_1$ (in outer valence), $4a_1$, and $3a_1$. The orbital contour maps of these three MO's confirm this three-

center interaction (Figure 14). The main interaction features are as follows:

$$7a_1: \quad Ni(3d_{z^2}) - N(2p) + O(2p)$$

$$4a_1: \quad Ni(3d_{z^2}) + N(2p) + O(2p)$$

$$3a_1: \quad Ni(3d_{z^2}) + N(2s) - O(2s)$$

The assignment of the inner-valence spectrum of CpNiNO is based on our ground-state Xα−SW calculation and the reported assignment for the NO inner-valence photoelectron spectrum (Table 4).[28] The NO bands are assigned to bands C ($2e_1$—NO 1π), D ($4a_1$—NO 3σ), E ($3a_1$—NO 2σ), and F (NO shake-up excitations). The reported IP for the NO 1σ band is about 40 eV, not covered in our spectrum. The Cp bands are assigned to bands A ($2e_2$), B ($3e_1$), D ($5a_1$, $1e_2$), E ($1e_1$), and G ($2a_1$).

(28) Freund, H.-J.; Kossmann, H.; Schmidt, V. *Chem. Phys. Lett.* **1987**, *137*, 425.

Conclusion

The study of the photoelectron spectrum for CpNiNO, using a combination of high-resolution He I spectrum, variable-energy spectra, and Xα−SW calculations, favors the assignment originally made by Hillier et al.[1] and disfavors the assignment which attributes a single band (band 2) to a vibrational member of the $5e_1$ MO.[5] The IP ordering from this assignment is consistent with the Xα ground-state orbital ordering and the orbital relaxation ordering derived from the sequence of Xα−SW Ni 3d compositions.

Acknowledgment. We are very grateful for the financial support of the NSERC (Canada) and for the continued assistance from the staff at the Aladdin Synchrotron. We thank Dr. J. C. Green for sending a draft of her group's paper and helpful discussions and thank Mr. Y. F. Hu and Dr. J. N. Cutler for their assistance. We also acknowledge the support of NSR Grant No. DMR-9212658 to the Synchrotron Radiation Center.

IC951013U